Impact of Interfacial Friction at the Ice-Bed Boundary on Glacier Sliding

J P Roldán-blasco, F. Gimbert, O. Gagliardini, A. Gilbert

JGR Earth Surface

RESEARCH ARTICLE
10.1029/2022JF007028

Special Collection:
Modeling in glaciology

Impact of Interfacial Friction at the Ice-Bed Boundary on Glacier Sliding

J. P. Roldán-Blasco[1], F. Gimbert[1], O. Gagliardini[1], and A. Gilbert[1]

[1]Univ. Grenoble Alpes, CNRS, INRAE, IRD, Grenoble INP, IGE, Grenoble, France

Abstract Current theories for describing glacier sliding over hard beds assume that basal drag is entirely due to normal forces acting on meter-scale bed roughness and neglect tangential friction at the ice-bed interface. However, this interfacial friction is likely to account for a significant proportion of basal drag in the presence of basal debris or cold ice, and may render current sliding theories inaccurate. The aim of the study is to evaluate if current sliding laws still apply in the presence of interfacial friction. We propose a simplified analytical model of glacier sliding controlled by both ice creep around bed irregularities, as proposed by Weertman (1957, https://doi.org/10.3189/s0022143000024709), and interfacial friction at the ice-bed boundary determined by Coulomb dependency. We show that reduced sliding speed from additional interfacial friction is mitigated by increased ice deformation near the bed, which occurs as a result of additional basal deviatoric stresses reducing the effective viscosity. We further generalize these results using a numerical model of glacier sliding over a sinusoidal bed, capable of simulating cavity formation and basal sliding with several formulations of interfacial friction. We find that the additional friction generally does not modify the form of previously proposed friction laws but significantly increases the maximum resistive shear stress of the bed. These results suggest that friction laws that are commonly used in ice-sheet models and whose parameters are empirically optimized, could be still used in circumstances where interfacial friction is non-negligible.

Plain Language Summary The existing models of glacier sliding over hard beds assume that resistance to flow at the base of glaciers, known as basal drag, entirely comes from deformation around a rough bed. This assumption is challenged by in-situ observations as well as models and laboratory experiments that show that drag between glaciers and their bed, due to debris, or other processes, can account for a significant proportion of the total resistance to flow. We develop a new model of glacier sliding that accounts for this process. We show that the friction at the ice-bed interface does not alter on the form of existing friction laws, providing theoretical support in their use to model large scale glacier dynamics.

Key Points:

- We provide new theoretical and numerical frameworks to describe the effect of ice-bed interfacial friction on glacier sliding
- Interfacial friction reinforces stress concentrations, which reduces the effective ice viscosity near the bed
- Sliding laws that account for interfacial friction have the same main characteristics as friction laws under pure sliding

Supporting Information:

Supporting Information may be found in the online version of this article.

Correspondence to:

O. Gagliardini,
olivier.gagliardini@univ-grenoble-alpes.fr

Citation:

Roldán-Blasco, J. P., Gimbert, F., Gagliardini, O., & Gilbert, A. (2025). Impact of interfacial friction at the ice-bed boundary on glacier sliding. *Journal of Geophysical Research: Earth Surface*, *130*, e2022JF007028. https://doi.org/10.1029/2022JF007028

Received 6 DEC 2022
Accepted 2 JUN 2025

Author Contributions:

Conceptualization: J. P. Roldán-Blasco, F. Gimbert, O. Gagliardini, A. Gilbert
Formal analysis: J. P. Roldán-Blasco
Investigation: J. P. Roldán-Blasco, F. Gimbert, O. Gagliardini, A. Gilbert
Methodology: J. P. Roldán-Blasco, F. Gimbert, O. Gagliardini
Software: J. P. Roldán-Blasco, O. Gagliardini
Writing – original draft: J. P. Roldán-Blasco, F. Gimbert, O. Gagliardini, A. Gilbert

1. Introduction

The dynamics of glaciers with a temperate base is strongly controlled by basal sliding (Doyle et al., 2018; Hooke et al., 1992; Maier et al., 2019). The conceptual view of glacier sliding over hard-bed is based on the seminal work of Weertman's (1957), in which he assumed that the sliding process is controlled by the enhanced deformation of ice around the bedrock irregularities. The relationship between basal shear stress and basal sliding speed, the so-called friction law, is defined at a meso-scale (few meters to several tens of meters) where basal shear stress results from the summation of normal stresses on micro-scale (decimetric to metric) obstacles (e.g., Budd et al., 1979; Fowler, 1986a; Gagliardini et al., 2007; Lliboutry, 1968; Schoof, 2005; Weertman, 1957). These obstacles induce stress concentrations within the ice, which causes reduction of the effective ice viscosity (Glen, 1955), enhances ice deformation and thus sliding. Further increase in sliding speed can occur as a result of the formation of pockets of water in the lee side of obstacles, referred to as cavities, which decrease the apparent sizes of bed irregularities and facilitate sliding (Fowler, 1986a; Gagliardini et al., 2007; Lliboutry, 1968; Schoof, 2005).

In the Weertman's (1957) conceptual model, the interface between the ice and the bed is assumed to be frictionless. Although such an assumption is justified in idealized circumstances of temperate glaciers in contact with a hard bedrock, where a thin layer of water is expected to form at the ice-bed interface (Weertman, 1957), it is unclear whether it remains valid under realistic conditions. Basal ice generally contains debris of various sizes, as shown in Figure 1 from a photograph taken in a natural cavity under the Glacier d'Argentière (France) (see also Alean et al. (1985) for a more general discussion on ice basal debris). These debris exert additional

Writing – review & editing: J. P. Roldán-Blasco, F. Gimbert, O. Gagliardini, A. Gilbert

Figure 1. Cavity under Argentière Glacier, French Alps. The debris cover visible at the base of the glacier varies in density during time. Photograph by Luc Moreau at http://www.moreauluc.com/.

shear resistance due to friction at the ice-bed interface, as confirmed by experiments in the laboratory (Zoet et al., 2013) and in the field (Iverson et al., 2003). In addition, patches of cold ice can be present even under generally temperate base conditions (Mantelli et al., 2019; Robin, 1976), causing friction at the ice-bed interface as observed in laboratory experiments under conditions close to the pressure-melting point (McCarthy et al., 2017). The occurrence of repeating basal shear ruptures, commonly referred to as stick-slip events and widely recorded from seismic observations, provide the evidence that interfacial friction is ubiquitous across large regions of glacier beds (Helmstetter et al., 2015; Köpfli et al., 2022; Lipovsky et al., 2019; Roeoesli et al., 2016; Wiens et al., 2008; Zoet et al., 2012). These events demonstrate the ability of glacier beds to accumulate stress and to suddenly release it. This process is unlikely occurs through viscous ice deformation; instead, it is more likely due to reaching a threshold in friction - a typical behavior of contacts between solid materials (Jaeger et al., 2007).

Experimental studies that investigated the effects of the interfacial friction on the glacier sliding, have primarily focused on the micro-scale mechanisms that control debris-bed friction (e.g., Cohen et al., 2005; Hansen & Zoet, 2019; Thompson et al., 2020) or cold ice-on-rock friction (e.g., McCarthy et al., 2017; Schulson & Duval, 2009). However, the influence of interfacial friction on the glacier sliding process, including enhanced ice deformation around meso-scale bed irregularities, has not been fully described. Previous studies have included interfacial friction by treating ice as a Newtonian fluid (Hallet, 1979, 1981; Morland, 1976) or by assuming that interfacial stress is low enough to not perturb the stress field within the ice (Fowler, 1986b; Iverson et al., 2019). These simplifications may lead to an underestimation of the control of interfacial friction on near-bed stress concentrations, which can influence sliding by changing the effective viscosity due to ice deformation around bed irregularities. Consequently, it is unclear how the interfacial friction affects the ice flow, and how these local effects manifest themselves in the functional form of the mesoscale sliding laws (i.e., on the scales of few meters to several tens of meters). Here, we address these questions by deriving a meso-scale friction law that takes into account interfacial friction at the ice-bed boundary and its effect through stress concentrations for a non-Newtonian ice rheology.

The manuscript is organized as follows: first, we briefly present the meso-scale friction laws and constitutive relationships that can be used to describe interfacial friction at the ice-bed boundary. We then analytically and numerically solve for a meso-scale friction law that includes these descriptions. We show that commonly used friction laws that do not account for interfacial friction can be extended to sliding with interfacial friction given appropriate scaling. Finally, we discuss our results in the broader context of predicting glacier basal velocity in large-scale models.

2. Background on Friction Laws

2.1. Meso-Scale Friction Under Perfect Sliding at the Ice-Bed Interface

There are several formulations of sliding laws that describe glacier sliding under perfect sliding assumption at the ice-bed interface. The first friction law was proposed by Weertman (1957) and takes the following form:

$$\tau_b = A_s^{-1/m} u_b^{1/m} , \tag{1}$$

where τ_b is the meso-scale averaged bed shear stress, u_b is the meso-scale averaged basal speed, m is a material exponent, and A_s is a sliding parameter. If enhanced ice deformation solely controls friction, as considered here, the exponent m is expected to be equal to the exponent n of the Glen's flow (see Equations 8 and 13). The sliding parameter A_s accounts for ice deformation enhancement within the basal boundary layer, which is a function of effective ice viscosity, itself strongly modulated by stress concentrations around bedrock bumps.

Another form of a sliding law was proposed by (Lliboutry, 1968), who identified that cavities may form in the lee side of bedrock bumps, smoothing the apparent roughness of the bed and resulting in faster sliding. We use the formulation proposed by Gagliardini et al. (2007) which was defined based on approximating numerical results as

$$\frac{\tau_b}{N} = C\left(\frac{\chi}{1+\alpha\chi^q}\right)^{1/n} , \text{ with } \chi = \frac{u_b}{(CN)^n A_s} , \ \alpha = \frac{(q-1)^{q-1}}{q^q} . \tag{2}$$

Where χ is a dimensionless parameter and C is a Coulomb-type friction coefficient that represents the maximum attainable basal shear stress $\tau_b = CN$, known as the Iken's bound (Iken, 1981). For $q = 1$, τ_b/N increases monotonically with u_b (Fowler, 1987; Schoof, 2005). For $q > 1$, the law is double-valued, that is, a given basal shear stress value corresponds to two velocity solutions, one in the velocity hardening regime (τ_b/N increases with u_b) and one in the velocity weakening regime (τ_b/N decreases with u_b). For $u_b \ll (CN)^m A_s$, Equation 2 predicts a behavior similar to that described by Equation 1. This law applies in three dimensions, as supported by laboratory experiments (Zoet & Iverson, 2015) and numerical simulations (Helanow et al., 2020). Though, the rate-weakening regime may no longer operate under realistic bed geometries (Helanow et al., 2021).

2.2. Micro-Scale Normal Stress Distribution and Resulting Friction at the Ice-Bed Interface

To explicitly prescribe interfacial friction in numerical simulations, the stress tensor $\boldsymbol{\sigma}$ and its normal and tangential components $\sigma_{nn} = \mathbf{n}\cdot\boldsymbol{\sigma}\mathbf{n}$ and $\sigma_{nt} = \mathbf{t}\cdot\boldsymbol{\sigma}\mathbf{n}$ (with $\mathbf{n}$ and $\mathbf{t}$ the normal, inward pointing, and tangential unit vectors, respectively) have to be solved for at any point of the ice-bed interface (see Figure 2b). Below we describe three sliding laws that may be used to solve for the interfacial friction term σ_{nt} under various considerations of the ice-bed interface properties. In Sections 4.2 and 4.4, we consider these sliding laws and test their impacts on the meso-scale friction.

The first law is based on the original hypothesis of Weertman that a water film exists and satisfies static equilibrium at the ice bed interface, that is, water pressure at the bed p_w equals normal stress $-\sigma_{nn}$ everywhere, such that local effective pressure

$$N_{loc} = -\sigma_{nn} - p_w \tag{3}$$

is zero. In this case, the ice pressure exerted on the clast is compensated by the water pressure surrounding the clast, such that interfacial friction is due to the buoyant weight of the clast and the ice-bed convergence velocity, which is non-zero as a result of ice stretching around obstacles and basal melting (Hallet, 1981; Iverson et al., 2019). Iverson et al. (2019) showed that, under constant effective pressure, the meso-scale (meter to tens of meters) interfacial drag does not vary significantly with basal speed. Indeed, any increase in interfacial drag due to an increase in sliding velocity is compensated by the growth of cavities that reduces the contact area between the ice and the bed, resulting in a more or less constant meso-scale interfacial drag. We approximate this result by considering that meso-scale interfacial drag is a constant function $\tau_f = c$, where the value of c depends on debris concentration and size, bed roughness characteristics and effective pressure (Iverson et al., 2019). We further assume that the local shear stress is uniform at the ice-bed interface such that:

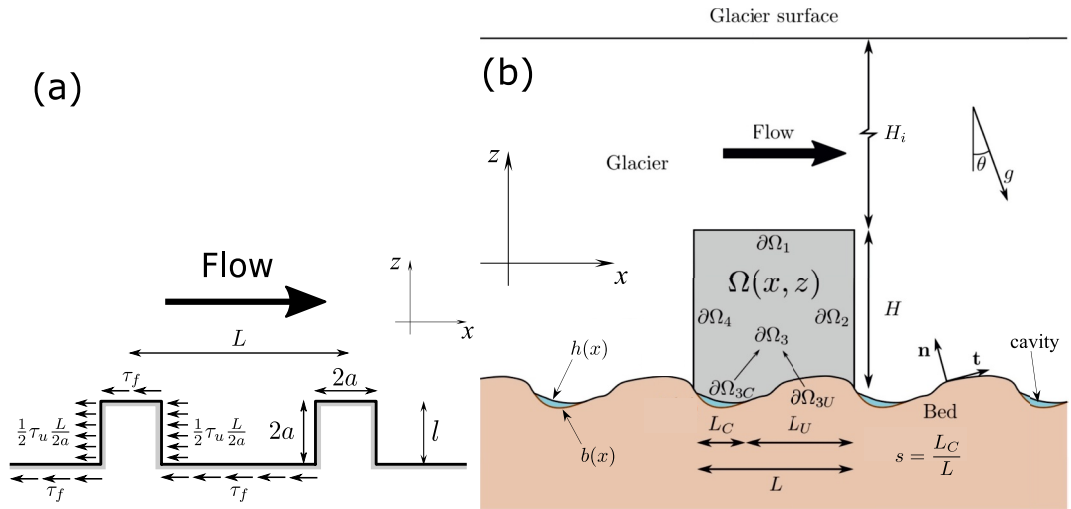

Figure 2. (a) Continuous version of the tombstone model with the additional considered stresses in the case of no cavity. (b) An example of a two-dimensional infinite glacier and the domain of interest Ω (in gray). The example shows a vaguely sinusoidal bed in brown with water-filled cavities in blue.

$$\sigma_{nt} = \frac{c}{1-s}\,, \tag{4}$$

where s is cavitated fraction of the bed (see Figure 2b). In our particular implementation, we impose the value of c and compute s using the numerical simulations. In the following, we refer to this approximation as the Hallet-like model.

The second law is based on the consideration that water does not play a role into friction at the ice-bed interface, as expected in the case of cold ice or of a debris cover in which clasts are not surrounded by water, as previously considered by Schweizer and Iken (1992). This debris layer must be highly concentrated and thick enough to keep the ice from converging toward the bed, while thin enough to follow the bedrock irregularities. In these cases, the dependency of local shear stress on the basal normal velocity is thus negligible and local shear stress is controlled by ice pressure, such that interfacial friction may be expressed through a Coulomb law as (McCarthy et al., 2017)

$$\sigma_{nt} = -\mu\sigma_{nn}\,. \tag{5}$$

where μ is the friction coefficient. Later we refer to this law as the Coulomb law.

The third law is based on the consideration that debris are surrounded by water at the ice-bed interface, but water pressure does not satisfy static equilibrium, that is $N_{loc} > 0$. This is expected if the water pressure is controlled by nearby cavities or channels, which have water pressures lower than overburden pressure as a result of cavity opening from sliding (Gagliardini et al., 2007; Lliboutry, 1959) or channel opening from wall melting (Röthlisberger, 1972). In these cases σ_{nt} is expected to depend on effective pressure N_{loc} as

$$\sigma_{nt} = \mu N_{loc}\,. \tag{6}$$

Later we refer to this law as the effective-pressure-driven denoted N-Coulomb law, and we assume a uniform water pressure everywhere equal to that in cavities.

3. Model Description

In order to investigate the effects of interfacial friction on the meso-scale glacier bed friction, we consider two modeling approaches. The first one is an analytical approach that follows the model by Weertman (1957) developed for a tombstone-like bed (Section 3.1). The second one is a numerical approach, in which we solve the Stokes equations describing ice flow over a sinusoidal bed shape (Section 3.2).

3.1. Analytical Model

The analytical model builds up on Weertman (1957) approach where bedrock irregularities are represented by cuboid protuberances equally spaced in all directions. In Weertman (1957) original work, the sliding law is calculated only from the normal stress applied to the vertical walls. We propose here an alternative approach where we add tangential stresses on horizontal surfaces in order to take into account interfacial friction at the ice-bed boundary.

We thus describe the bed elevation $b(x)$ as a rectangular function made of protuberances of height $2a$ separated between each other by a distance L, with roughness $r = a/L$ (see Figure 2a). To keep it consistent with the two-dimensional flow assumption, we consider infinitely large bumps in the transverse direction, contrary to Weertman (1957) who considered bumps of equal width and height. We further assume that (a) viscous drag operates on the vertical sides and interfacial drag on the horizontal sides of the bumps, and (b) longitudinal and shear stresses are estimated to be on the order of the additional stresses induced by the presence of bumps and interfacial drag. Assuming a two-dimensional plane strain flow over square obstacles of height $2a$ and roughness $r = a/L$ (see Figure 2a), deviatoric stresses including the contributions of viscous drag τ_u and interfacial friction τ_f can be expressed as (Cuffey & Paterson, 2010):

$$\begin{aligned} \tau_{xx} &= \frac{1}{2}\tau_u \frac{L}{2a},\ \tau_{zz} = -\tau_{xx}, \\ \tau_{xz} &= \tau_f, \\ \tau_E &= \left(\frac{L^2}{16a^2}\tau_u^2 + \tau_f^2\right)^{\frac{1}{2}}, \end{aligned} \tag{7}$$

where τ_E is the effective deviatoric stress. With the constitutive law of ice deformation described as

$$\dot{\varepsilon}_{ij} = A\tau_E^{n-1}\tau_{ij}, \tag{8}$$

where A is the creep parameter, the above Equation 7 gives the following expressions for the strain-rate components:

$$\dot{\varepsilon}_{xx} = \frac{A}{4}\frac{L}{a}\left(\frac{L^2}{16a^2}\tau_u^2 + \tau_f^2\right)^{\frac{n-1}{2}}\tau_u \ \text{ and } \ \dot{\varepsilon}_{xz} = A\left(\frac{L^2}{16a^2}\tau_u^2 + \tau_f^2\right)^{\frac{n-1}{2}}\tau_f\,, \tag{9}$$

where $\dot{\varepsilon}_{xx}$ is the longitudinal strain-rate and $\dot{\varepsilon}_{xz}$ the shear strain-rate, both dependent on τ_u and τ_f.

The sliding velocity is estimated by integrating $\dot{\varepsilon}_{xx}$ and $\dot{\varepsilon}_{xz}$ over relevant horizontal and vertical distances, which we both consider equal to $2a$ (see Figure 2). Assuming the strain rates are constant over these distances, the sliding velocity can be calculated as

$$u_b = \left(\dot{\varepsilon}_{xx} + 2\dot{\varepsilon}_{xz}\right)2a\,. \tag{10}$$

Rewriting Equation 9 to include the roughness $r = a/L$, we obtain

$$u_b = A\left(\frac{\tau_u^2}{16r^2} + \tau_f^2\right)^{\frac{n-1}{2}}\frac{\tau_u}{4r}2a + A\left(\frac{\tau_u^2}{16r^2} + \tau_f^2\right)^{\frac{n-1}{2}}4a\tau_f\,. \tag{11}$$

we define the interfacial drag ratio $T = \tau_f/\tau_b$ such that $\tau_u = (1-T)\tau_b$, $\tau_f = T\tau_b$ and Equation 11 reduces to

$$u_b = A\left(\frac{(1-T)^2}{16r^2} + T^2\right)^{\frac{n-1}{2}}\left(\frac{1-T}{4r} + 2T\right)2a\tau_b^n = A_f(T)\tau_b^n\,, \tag{12}$$

Table 1
Comparison Between Theoretical Basal Drag Upper Bound (See Appendix A) and Computed Basal Drag Upper Bound C_f for the Tests Carried out in Section 4.4 Over a Sinusoidal Bed of Roughness $r = 0.05$

Interfacial friction	Theoretical C_f	Computed C_f	Notes
Hallet	$C + \tau_f/N = 0.298$	0.320	$\tau_f = 50$ kPa and $N = 700$ kPa.
Coulomb	$C + (1-s)\mu + s\mu\bar{p}_i/N = 0.312$	0.331	$s = 0.693$ and $N = 634$ kPa.
N-Coulomb	$C + \mu = 0.304$	0.301	–

Note. We set $\tau_f = 50$ kPa in the Hallet-like model and $\mu = 0.05$ in both Coulomb and N-Coulomb models.

with $A_f(T)$ a function of T.

Our result is consistent with the original solution from Weertman (1957) (Equation 1) which can be retrieved by setting $T = 0$ in the previous equation, in which case we have

$$u_b(T=0) = \frac{A}{(4r)^n} 2a\tau_b^n = A_s\tau_b^n \,, \tag{13}$$

using Equation 13, the sliding parameter with interfacial drag $A_f(T)$ in Equation 12, relative to the sliding parameter without interfacial drag A_s, is obtained as

$$A_f(T)/A_s = \left((1-T)^2 + 16r^2T^2\right)^{\frac{n-1}{2}}((1-T) + 8rT) \,. \tag{14}$$

In this equation, the first term that depends on the flow-law exponent n, represents the effects of nonlinear ice rheology; the second term sets the relative contribution of the bed roughness and the interfacial drag to the sliding velocity. If the roughness value $r < 1/4$, the first term is always less than one. Consequently, for a given value of T the first term becomes smaller as the flow-law exponent n becomes larger. As a result, the ratio of the sliding parameter with interfacial drag $A_f(T)$ to the sliding parameter without interfacial drag A_s becomes smaller. This indicates that the non-linearity of the ice rheology modulates the effects of the interfacial drag on the sliding velocity.

3.2. Numerical Model

We consider a two-dimensional infinitely long glacier of average thickness $H + H_i$ and surface slope θ contained in the $x - z$ plane and flowing over a sinusoidal periodic bed of elevation $z = b(x)$ and period L (see Figure 2b and Table 1 for the notation definition). The bottom boundary of the ice is given by the periodic function $z = h(x) \geq b(x)$. A cavity can form at the locations where $h > b$. We focus on a subdomain Ω of length L and height H (Figure 2b).

Periodic boundary conditions are applied on right and left sides ($\partial\Omega_2$ and $\partial\Omega_4$). Above $\partial\Omega_1$, we assume that the ice flow is undisturbed by the irregularities of the bed, such that at $z = H$ the stress and velocity fields are uniform. Far field conditions are applied on the top boundary $\partial\Omega_1$ and correspond to the overburden ice pressure of the ice column of height H_i over the modeled domain and uniform horizontal velocity $\bar{u}_i$, such that

$$\sigma_{yy}(x,H) = \bar{p}_i = -\rho_i g H_i \cos(\theta) \quad \text{and} \quad u(x,H) = \bar{u}_i \quad \text{on } \delta\Omega_1 \,. \tag{15}$$

The domain length can be subdivided into two parts, $L = L_C + L_U$, each corresponding to $\partial\Omega_{3C}$ and $\partial\Omega_{3U}$ respectively. In the domain Ω, the Stokes flow equations for incompressible ice (momentum and mass conservation) are solved to calculate the ice velocity $\mathbf{u}(x,z)$ and pressure $p(x,z)$:

$$\nabla\cdot\boldsymbol{\sigma} = \mathbf{0}, \nabla\cdot\mathbf{u} = 0 \,. \tag{16}$$

Note that the effect of gravitational force is taken into account by the stress condition $\bar{p}_i$ at the top boundary and is neglected in the domain Ω given its small contribution compared to $\bar{p}_i$.

The water pressure in the cavity, p_c is uniform. At the cavitated interface $\partial\Omega_{3C}$ we impose normal stress equal to the cavity water pressure and that the tangential stress is null, that is:

$$\sigma_{nn}(x,h) = -p_c \quad \text{and} \quad \sigma_{nt}(x,h) = 0 \quad \text{on } \delta\Omega_{3C}\,. \tag{17}$$

At the uncavitated interface $\partial\Omega_{3U}$, the conditions are the following: ice does not penetrate the bed and experiences local shear stress, that is,

$$\mathbf{u}(x,h)\cdot\mathbf{n} = 0 \quad \text{and} \quad \sigma_{nt}(x,h) = \sigma_{nt} \quad \text{on } \delta\Omega_{3U}\,, \tag{18}$$

with σ_{nt} given by either Equations 4, 5 or 6.

We use the finite element model Elmer/Ice (Gagliardini et al., 2013), following the approach of Gagliardini et al. (2007). The Stokes Equation 16, assuming $n = 3$ in Equation 8, are solved together with the free surface evolution equation for the ice bottom surface $h(x)$

$$\frac{dh}{dt} + u\frac{dh}{dx} - w = 0 \quad \text{on } \delta\Omega_3\,, \tag{19}$$

with the boundary conditions given by Equations 15, 17 and 18 and the periodicity of $\mathbf{u}$ and h on the two lateral boundaries.

The impenetrability condition $h \geq b$ is enforced using a method of imposed Dirichlet condition based on the residual of the free surface equation (Gagliardini et al., 2013). At each timestep, the contact condition between the ice and the bed is tested for each node on the bed. If the normal component of the residual of the Stokes equations is smaller than the normal force exerted by the water pressure, then the node is released, that is boundary conditions (Equation 18) apply for this node instead of Equation 17. For the numerical simulations, the bed elevation is a sinus function of amplitude a,

$$b(x) = a\sin\left(\frac{2\pi x}{L}\right). \tag{20}$$

The numerical domain is a regular mesh of bi-linear quadrilateral elements, vertically refined toward the bottom boundary, with $L = H = 10$m. Note that since we keep the domain length fixed, we modify bed roughness by changing a.

The model is run until the cavity size reaches steady-state for different given values of water pressure p_c between 0 and $0.8\bar{p}_i$ with increments of $0.01\bar{p}_i$. We assume $\bar{p}_i = 1.77$ MPa (200 m of ice) and top velocity $\bar{u}_i = 150$ m a^{-1}. The friction law is inferred from spatially averaged variables u_b, τ_b, τ_f and N which are calculated by integrating the tangential velocity vector and the normal stress vector over the bottom ice interface for each steady state solution.

4. Results

This section describes the results of the analytical and numerical models presented in the previous section. We start with the analysis of the analytical solutions obtained in Section 3.1 and then present the results of the numerical model described in Section 3.2 for three different interfacial friction laws.

4.1. Analytical Solution

The influence of interfacial friction is quantified in relation to the total drag through the ratio $T = \tau_f/\tau_b$. This ratio reflects the proportion of the basal drag that is accommodated by interfacial friction. High values of T reflect significant friction at the ice-bed interface, due to high debris content or partially frozen conditions. The quantity $(1 - T)$ reflects the proportion of basal drag accommodated by normal forces acting on the bed roughness. In this section, we analyze how the apparent sliding coefficient $A_f(T)$ (Equation 14) varies with T under variable roughness r or Glen's exponent n. We consider bedrock with a single roughness wavelength, thus r is simply defined as the aspect ratio between the amplitude a and length L of the bedrock bumps (see Figure 2).

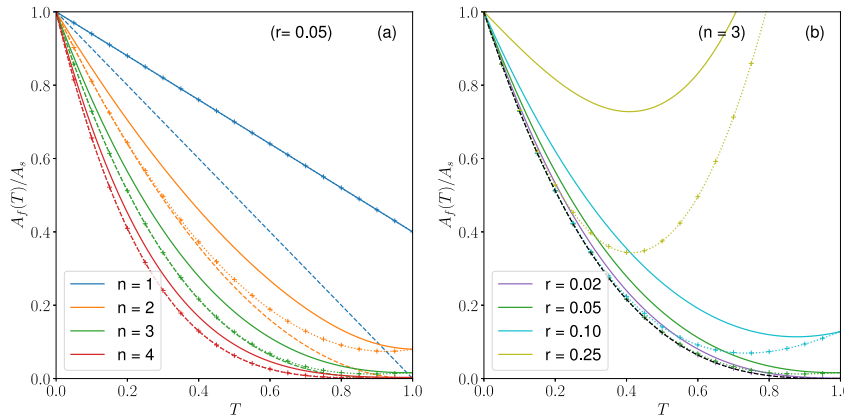

Figure 3. Dependence of $A_f(T)/A_s$ as a function of $T = \tau_f/\tau_b$ for (a) different Glen's law exponents n and (b) different roughnesses r. The solid lines represent the full expression of Equation 14, the dotted lines with crosses represent the solution neglecting effective viscosity feedbacks Equation 21 and the dashed lines the low roughness approximation Equation 22 when $r \to 0$ (black line in panel (b)).

We show that, for a given roughness of $r = 0.05$, the sliding parameter ratio $A_f(T)/A_s$ (Equation 14) is a decreasing function of T but also decreases with n regardless of T (Figure 3a). It means that for a given stress, sliding velocity will always decrease with increasing interfacial friction and also that its effect is stronger with increasing non-linearity in the Glen's law. For roughness greater than $8^{-1/n} \times 16^{(1-n)/(2n)}$ (i.e., $r = 0.198$ with $n = 3$), the apparent sliding parameter $A_f(T)$ becomes larger than A_s (Figure 3b), indicating that our simplified analytical solution does not apply in this range of very high roughness. Note that the exact value of this upper limit on r depends on the arbitrary choice $l = 2a$ made in Equation 10.

If we were to ignore the contribution of interfacial drag τ_f to the effective stress τ_E when estimating $\dot{\varepsilon}_{xx}$, and the contribution of viscous drag τ_u when estimating $\dot{\varepsilon}_{xz}$, we would have $\dot{\varepsilon}_{xx} = A(L/(4a))^n \tau_u^n$ and $\dot{\varepsilon}_{xz} = A\tau_f^n$, which gives

$$A_f(T)/A_s = (1-T)^n + 2(4rT)^n \,. \tag{21}$$

The difference between the full Equation 14 and this Equation 21 is shown in Figure 3a (solid lines vs. dotted lines with crosses respectively). It shows that, for a non-linear ice rheology $n > 1$, the decrease in the ratio $A_f(T)/A_s$ with T would be stronger without the influence of τ_f on $\dot{\varepsilon}_{xx}$ through its effect on the effective viscosity. In practice, this means that interfacial friction exerts a negative feedback on ice effective viscosity, enhancing deformation and partially mitigating the decrease in sliding speed. The larger is n (and the lower r), the weaker is this feedback.

For a very smooth bed ($r \to 0$), Equation 14 simplifies to

$$A_f(T)/A_s = (1-T)^n \,, \tag{22}$$

as proposed by Fowler (1986b). As shown in Figure 3a for $r = 0.05$, the low roughness approximation (dashed lines) is inaccurate for $n < 4$ but provides a good approximation for $n = 4$. For $n = 3$, the approximation remains accurate for roughnesses up to 0.02 with an underestimation of the sliding velocity by less than 10% (Figure 3b). A roughness of $r = 0.02$ corresponds to bedrock bumps of 20 cm amplitude with 10 m wavelength, which is significantly lower than generally observed on glacier beds (Helanow et al., 2021), making the low roughness approximation unlikely to be applicable in the real case.

4.2. Numerical Simulations

Here we present results from the numerical simulations over the sinusoidal bed using the N-Coulomb law to describe interfacial friction (Equation 6) and adopting $n = 3$ in Equation 8. Results with the two other interfacial friction laws are presented in the next section. In order to represent friction laws in a one-dimensional space, while

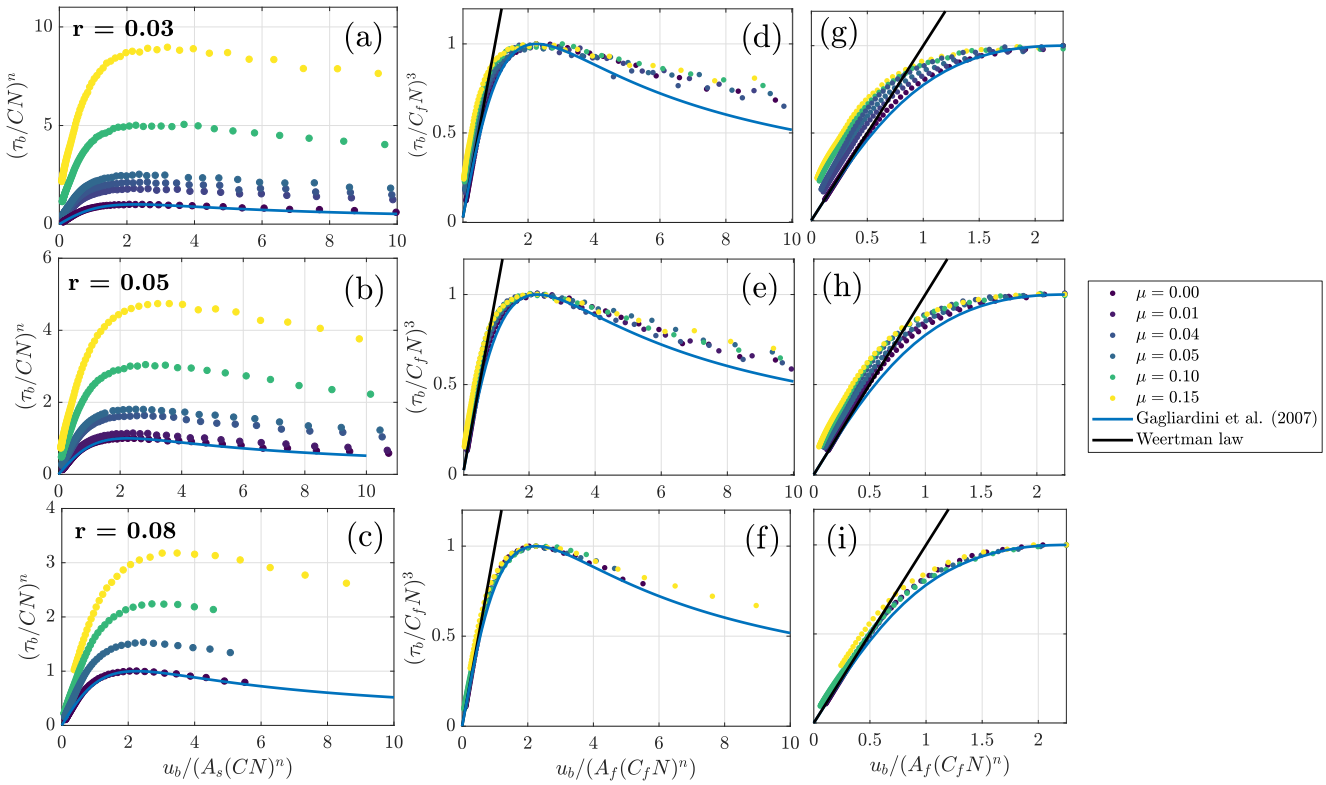

Figure 4. Friction laws obtained numerically for a sinusoidal bed of roughness $r = 0.03$ (panels a, d, and g), $r = 0.05$ (panels b, e,and h) and $r = 0.08$ (panels c, f, and i) and different values of μ. For each roughness, the panels (a, b, and c) use C and A_s as scaling parameter, the panels (d, e, and f) C_f and A_f as scaling parameter and the panels (g, h, and i) are a zoom of the panels (d, e, and f) respectively. The solutions from Weertman (1957) and Gagliardini et al. (2007) are shown as black and blue lines respectively.

it depends on the two variables u_b and N, we show results as functions of normalized bed shear stress τ_b/CN and velocity $u_b/As(CN)^n$ with $n = 3$. We present three realistic bed roughness $r = 0.03$, 0.05, and 0.08 for μ varying between 0 and 0.15 as typically expected for interfacial friction at the glacier base (Cohen et al., 2005).

As Figures 4a–4c illustrate, the relationships between the basal shear and sliding velocity, the friction laws, are such that for low values of the sliding velocities the basal shear increases until the peak value is reached (i.e., rate-strengthening regime) and for larger values of the sliding velocities it decreases (i.e., rate-weakening regime). The peak stress is sensitive to the value of μ with increasing value for higher μ. The values of A_s and C for each roughness r are obtained from the simulation with $\mu = 0$ and assuming that $A_s = u_b(p_c = 0)/\tau_b^n(p_c = 0)$ and $C = \max(\tau_b/N)$. We find that the simulation with $\mu = 0$ are best fitted using the Gagliardini et al. (2007) law (Equation 2) with $q = 1.8$ and $C = 2\pi kr$ ($k = 0.8$). We note that the value of k is in agreement with the value obtained by (Gagliardini et al., 2007) and is intrinsically linked to the sinusoidal shape of the bedrock in our experiment. It may be different for a real three-dimensional bed with multiple wavelengths.

We investigate how the friction law in Equation 2 can be generalized for the case $\mu > 0$ by evaluating, for each value of μ; whether an appropriate tuning of its parameters $C = C_f$ and $A_s = A_f$ allows a reasonable fit of the friction laws shown in Figures 4a–4c. We find that the numerical results can be fitted fairly well with Equation 2 using different given values of C_f and A_f for each values of μ and r (Figures 4d–4i). To compute these parameters, we impose that all curves reach the peak at the same point $u_b/\left(A_f\left(C_fN\right)^n\right) = \chi_M$ and $\tau_b/\left(C_fN\right) = 1$ where the value of χ_M is a unique function of $q = 1.8$ given by $\chi_M = \frac{q}{q-1} = 2.25$ (Gagliardini et al., 2007).

We evaluate how C_f can be expressed as a function of μ and r by determining a theoretical upper bound for shear stress based on the force balance considerations (see Appendix A) and find that $C_f = C + \mu$ (Equation A14). Using $C = 2\pi rk$ as suggested by Gagliardini et al. (2007) and this study we thus have:

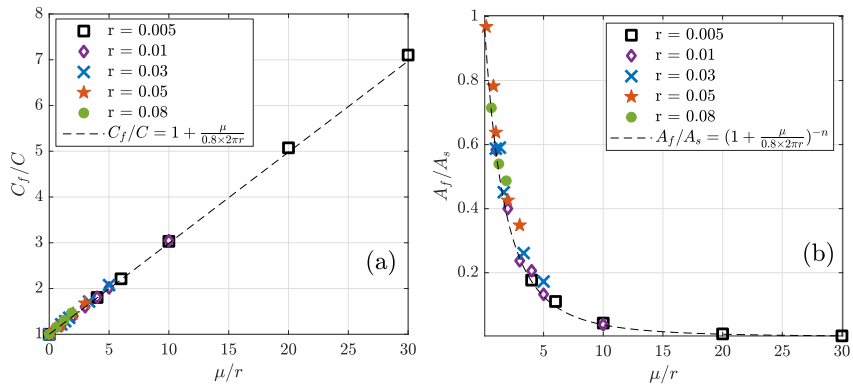

Figure 5. Normalized scaling parameters (a) C_f/C and (b) A_f/A_s as a function of μ/r derived from the numerical simulations for different roughness.

$$\frac{C_f}{C} = 1 + \frac{\mu}{2\pi k r}. \tag{23}$$

using our definition of $u_b/\left(A_f\left(C_f N\right)^n\right) = \chi_M$ and assuming that the weakening regime is always reached for the same values of (u_b, N), independently of μ, we have $A_f/A_s = (1 + \mu/C)^{-n}$. We thus expect A_f/A_s to be also a function of μ/r of the form

$$\frac{A_f}{A_s} = \left(1 + \frac{\mu}{2\pi k r}\right)^{-n}. \tag{24}$$

we verify this theoretical results by plotting the ratios C_f/C and A_f/As obtained numerically as a function of μ/r (Figure 5). We find that both C_f and A_f are indeed unique functions of μ/r that can be accurately fitted by the two relationships provided earlier (Equations 23 and 24).

4.3. Improved Formulation of the Sliding Law With Interfacial Friction

Although Equation 2 gives an acceptable estimation of the friction law with interfacial drag (Figure 4, using the proposed values of C_f and A_f), it was not derived to account for interfacial friction and some aspects of the friction behavior are not well captured, especially when interfacial friction becomes large ($\mu \approx C$) (Figures 4g and 4h). In particular, with interfacial drag, sliding occurs only above a certain stress threshold such that the basal shear stress does not vanish anymore when the sliding velocity tends to zero. Also, the different laws do not exactly match the Weertman law at low velocity as assumed in Equation 2. This is because A_f is no longer a constant as it depends on $T = \tau_f/\tau_b$ (see Section 3.1).

In order to improve the functional form of the friction law in the presence of interfacial drag and to resolve the limitations mentioned above, we propose to modify the original formulation of Gagliardini et al. (2007) by adding a term that takes into account the interfacial drag, which we expect to be of the form $f(r)\mu N$ such that

$$\tau_b = CN\left(\frac{\chi}{1 + \alpha\chi^q}\right)^{1/n} + f(r)\mu N, \text{ with } \chi = \frac{u_b}{A_f\left(C_f N\right)^n} \tag{25}$$

For the sinusoidal bed considered in this study, we find that, with $f(r) = (1 + C(r)/2)$, Equation 25 provides a more accurate estimate of the basal shear stress τ_b, especially at low roughness (see Figure 6). It also satisfies the condition that the basal shear stress τ_b does not necessarily vanish for $u_b = 0$.

4.4. Comparison Between the Three Interfacial Friction Laws at the Ice-Bed Boundary

We apply a similar approach to the two other micro-scale descriptions of interfacial friction given by the Hallet-like (Equation 4) and Coulomb (Equation 5) models. We do so for a fixed roughness value of $r = 0.05$, which

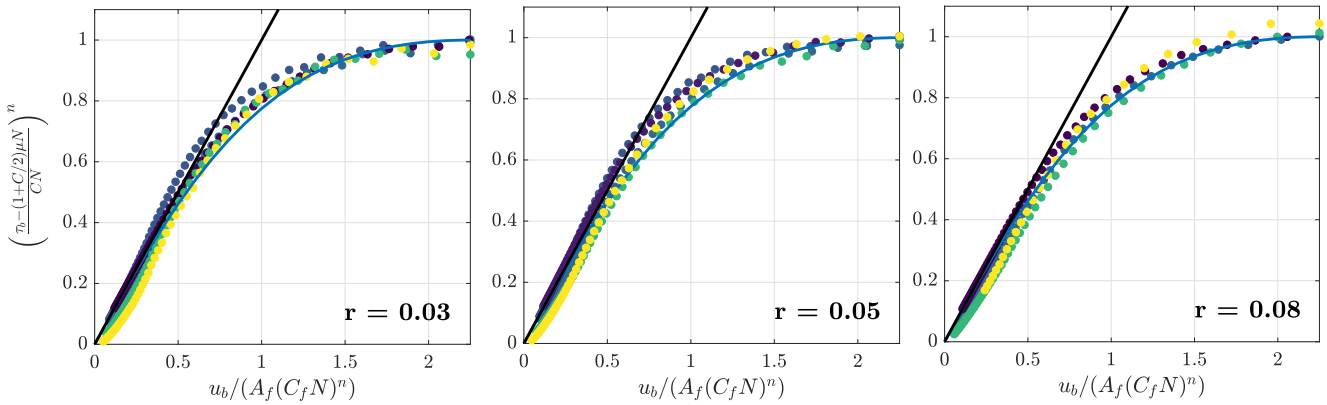

Figure 6. Friction laws obtained numerically for three different roughness r and scaled according to Equation 25 with $f(r) = (1 + C/2)$ (blue line). The dot colors refer to the different values of μ (same as in Figure 4) and the black line is the Weertman law.

would represent a bedrock bump of 1 m amplitude over a distance of 20 m. We used a fixed value for the interfacial drag $\tau_f = 50$ kPa for the Hallet-like model and a friction parameter $\mu = 0.05$ for the Coulomb model.

As Figure 7 illustrates, the Hallet-like and Coulomb models exhibit a behavior similar to that of the N-Coulomb models (Equation 6) presented in the previous section. The values of $C_f = \max(\tau_b/N)$ are also found to match quite well the theoretical values obtained in Appendix A (see Table 1). The largest difference between the models is seen in the magnitude of the local shear stress distribution, which can differ by a factor of 2 between the Hallet-like and the two Coulomb models (see Figures S1–S3 in Supporting Information S1).

5. Discussion

5.1. Application of Friction Laws in Large Scale Models

Basal ice, including debris or frozen conditions, is expected to cause non-negligible friction at the ice-bed interface, which may challenge the applicability of friction laws developed under the assumption of perfect sliding that are used in current glacier and ice-sheet prediction models. The analytical and numerical analyses conducted in this study allowed us to quantify the effects of interfacial friction on the basal sliding of glaciers. We find that for roughness values typically greater than $r = 0.05$, the effect of interfacial friction can be taken into account simply by adjusting the parameters of previously established friction laws under perfect sliding at the ice-bed boundary (Gagliardini et al., 2007). Such roughness values are expected for real glacier beds (Helanow et al., 2021), suggesting that the friction laws widely used in large-scale ice-sheet models (e.g., Goelzer et al., 2020; Seroussi et al., 2020) could still be used in circumstances where interfacial friction is not negligible. The main effect of interfacial drag is to increase the maximum bed shear stress that can be supported by the bed so that the proposed values of C, based on the assumption of perfect sliding, may be underestimated in previous studies (Helanow et al., 2021). This can be of primary importance for large-scale modeling, since small changes in stress near this point result in large changes in velocity, making simulations of the ice flux highly sensitive to this parameter (Brondex et al., 2019).

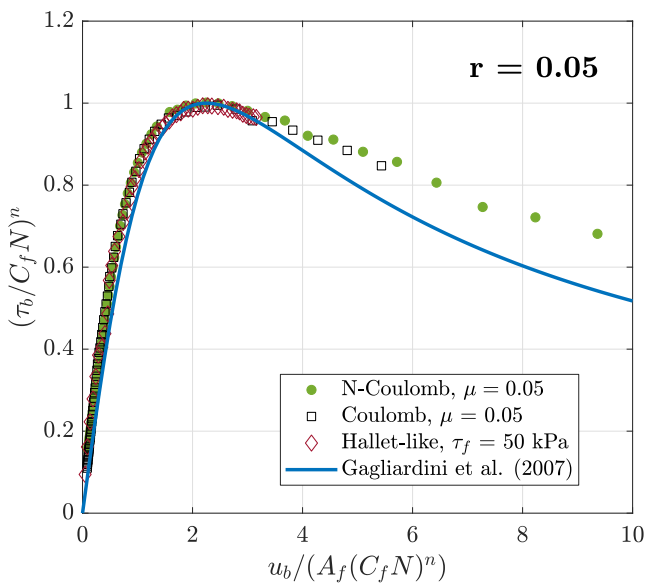

Figure 7. Friction laws obtained numerically for a sinusoidal bed with $r = 0.05$ and using the three different local shear stress laws described in Section 2.2. We set $\tau_f = 50$ kPa in the Hallet-like model and $\mu = 0.05$ in both Coulomb and N-Coulomb models. The blue line shows the solution from Gagliardini et al. (2007).

For roughness values lower than $r = 0.05$, the Gagliardini et al. (2007) approximation underestimates the shear stress at low velocities because, under Coulomb-type interfacial friction, a minimum shear stress must be applied before sliding starts to occur (Figure 4). We show that in this case the contribution of interfacial drag should be accounted for by a separate term, leading to Equation 25, which better captures this behavior (Figure 6). The existence of a stress threshold means that small changes in stress, such as

those associated with changes in ice thickness, can lead to significant changes in the flow regime by suddenly triggering sliding when the threshold is reached.

Finally, at low sliding velocities where cavitation does not occur, the form of friction no longer follows an exact Weertman-type power-law scaling (Figure 6). Instead, the basal shear stress depends not only on sliding velocity but also on effective pressure through its influence on interfacial friction (see Section 4.1). Nevertheless, the numerical results indicate that the deviation from the Weertman law is never very large and that this law for friction without cavitation may remain appropriate within a certain range of uncertainty (Figure 6).

5.2. Identifying the Signature of Interfacial Friction in Field Observations

Our finding that the friction law remains generally similar with or without interfacial friction complicates the identification of the contribution of interfacial shear stress based on inference of bed shear stress τ_b versus sliding velocity u_b at the natural scale (e.g., Gimbert et al., 2021). A possible solution to identify this contribution would be to compare field estimates of A_s and C with those obtained in accurate flow simulations over detailed three-dimensional glacier beds (Helanow et al., 2021), as discrepancies in parameter values could result from interfacial friction. Based on numerical simulations performed on real beds, Helanow et al. (2021) reported values of C between 0.11 and 0.2 that can be compared with values of $C = 0.4$ and $C = 0.6$ reported by (Gimbert et al., 2021; Togaibekov et al., 2024) respectively, based on the field observations at the Argentière Glacier (Mt Blanc range). These differences would lead to an average value of $\mu = 0.35$ which is much higher than previously proposed (Cohen et al., 2005). However, it could be that the value of C found by Helanow et al. (2021) is underestimated due to the limited domain size of their simulations, which neglect part of the roughness range capable of supporting higher stresses. Another possibility is that the Argentière Glacier bed is too different from those considered in Helanow et al. (2021) being in the deglaciated areas. This illustrates the difficulty in evaluating the amount of interfacial friction from field observations.

An alternative way of constraining interfacial friction could be to use our finding that interfacial friction increases near-bed stress concentrations and deformation rates. Borehole deformation measurements (Roldán-Blasco et al., 2025) could thus provide an indication of interfacial friction, which could be quantified by detailed modeling constrained by the observed deformation rate.

5.3. Study Limitations

Our results have been obtained under the assumption of steady-state conditions where the cavities are in equilibrium with the sliding velocity and effective pressure. Allowing for the transient response of the cavities would lead to a more complex behavior of the basal shear stress evolution in response to the transient changes in effective pressure. Friction laws that account for the transient evolution of the cavities have already been developed and include a third variable describing the cavitation state in addition to sliding velocity and effective pressure (Gilbert et al., 2022; Thøgersen et al., 2019; Togaibekov et al., 2024). However, they remain to be tested in microscale numerical experiments such as those carried out under this study.

Another limitation of our study is the application to a simplified 2D sinusoidal bed, which likely reduces the complexity of the local stress field that prevails in a realistic 3D bed geometry. The validity of our results should therefore be tested for other geometries, both two- and three-dimensional.

Finally, numerical results have been obtained for a Glen exponent $n = 3$ and the validity of Equations 23 and 24 should be tested against numerical results for $n \neq 3$.

6. Conclusions

In this study, we have investigated the effects of interfacial friction at the glacier-bed interface caused by the presence of debris or cold patches. In our analysis we have used two models - a simplified analytical model and a numerical model. The analytical model is based on a seminal study of Weertman (1957). The results of the analytical model suggest that the presence of interfacial friction caused stress concentration in the ice that, due to the ice non-Newtonian rheology, reduces its effective viscosity. This viscosity reduction represents a negative feedback as it limits slowdown of the ice sliding velocity. Using the results of our numerical model, we construct a functional dependence of the basal shear stress as a function of water pressure and sliding velocity by simulating the ice deformation in the vicinity of the bedrock with the sinusoidal shape. Our results show that the presence of

the interfacial friction does not change the general form of sliding laws. Our results also show that the maximum value of the basal shear stress (*CN*) is determined by the effects of the maximum adverse slope of the bedrock and the magnitudes of the interfacial friction coefficient μ. They also suggest that the estimates of *CN* obtained in studies that neglected the interfacial friction have lower values compared to those obtained here. Additionally, we find that the sliding parameter A_s also depends on the interfacial friction, and is no longer only a function of ice rheology and bed roughness. We point out that our results are obtained for two-dimensional settings (one horizontal and one vertical dimensions). Testing them in three-dimensional configurations is a subject of future research.

Appendix A: The Effect of Interfacial Friction on the Upper Bound of Bed Shear Stress

In order to evaluate the effect of non-zero interfacial friction on the upper bound for shear stress, known as Iken's bound (Iken, 1981) and set by the friction coefficient C in Equation 2, we integrate the vertical and horizontal forces over the bottom boundary following Schoof (2005). We hereafter consider the convention of negative stresses for compression, and normal and tangential vectors **n** and **t** oriented as drawn in Figure 2b. Basal drag and overburden pressure must be balanced by reaction forces at the bottom boundary $\partial\Omega_3$, such that

$$\left(-\tau_b, \bar{p}_i\right) = -\frac{1}{L}\int_{\partial\Omega_3} \boldsymbol{\sigma}\mathbf{n} ds\ , \tag{A1}$$

with ds the curvilinear coordinate along boundary $\partial\Omega_3$. We note $h' = dh/dx$ the local slope of the ice bottom boundary, such that $\mathbf{n} = \left(1 + h'^2\right)^{-1/2}(-h', 1)$ and $ds = \left(1 + h'^2\right)^{1/2} dx$. Projecting Equation A1 into the horizontal and vertical direction, and considering that $\sigma_{nt} = 0$ on $\partial\Omega_{3C}$ gives

$$\tau_b = \frac{1}{L}\int_L h'\left(-\sigma_{nn}\right) dx + \frac{1}{L}\int_{L_U} \sigma_{nt}\ dx, \tag{A2}$$

and

$$\bar{p}_i = \frac{1}{L}\int_L -\sigma_{nn} dx - \frac{1}{L}\int_{L_U} h'\sigma_{nt}\ dx\ . \tag{A3}$$

Equation A2 gives the balance of horizontal force at the ice base, with the basal drag τ_b resulting from the sum of the viscous drag τ_u, inherited from normal stresses on bedrock bumps, with the interfacial drag τ_f, inherited from non-zero local shear stress, where τ_u and τ_f are defined as

$$\tau_u = \frac{1}{L}\int_L h'\left(-\sigma_{nn}\right)\ dx \text{ and } \tau_f = \frac{1}{L}\int_{L_U} \sigma_{nt}\ dx\ . \tag{A4}$$

Shear stress partitioning between viscous and interfacial drags can be quantified through the interfacial drag ratio T as

$$T = \frac{\tau_f}{\tau_b},\ 0 \le T \le 1\ . \tag{A5}$$

In the case of no interfacial drag, the upper bound for shear stress is obtained by assuming that $-\sigma_{nn}$ cannot be lower than a critical water pressure value p_w (Schoof, 2005). Re-writing Equation A2 as

$$\tau_b = \frac{1}{L}\int_L h'\left(-\sigma_{nn} - p_w\right) dx + \frac{1}{L}\int_L h' p_w dx + \frac{1}{L}\int_{L_U} \sigma_{nt}\ dx. \tag{A6}$$

And considering that the terms $\frac{1}{L}\int_L(-\sigma_{nn} - p_w)\,dx = \frac{1}{L}\int_L N_{loc}dx = N$ and $\frac{1}{L}\int_L h' p_w dx$ vanish under periodic boundary conditions, the upper bound for τ_u is obtained under the condition $N_{loc} > 0$ such that

$$\tau_u \leq \frac{\sup(h')}{L}\int_L N_{loc}dx = \sup(h')\,N. \tag{A7}$$

In that case C depends solely on the slope of the ice bottom boundary h' and verifies the condition

$$C = \max(\tau_u/N) \leq \sup(h')\,. \tag{A8}$$

Because $\sup(h') \leq \sup(b')$, this bound even accounts for the decrease of τ_u/N as soon as the maximum bed slope $\sup(b')$ has been drowned by the cavity, and is therefore even stricter than the original Iken's bound (Iken, 1981). It also explains the weakening regime induced by cavity opening and included in Equation 2.

We consider the case of interfacial drag by adding τ_f to both sides of the inequality Equation A7, which gives:

$$\tau_b \leq \sup(h')\,N + \tau_f. \tag{A9}$$

we obtain an upper bound set by C_f as

$$C_f = \max(\tau_b/N) \leq \sup(h') + \tau_f/N\,. \tag{A10}$$

In the case of the Hallet-like constitutive law (Equation 4), we have

$$C_f \leq \sup(h') + c/N\,. \tag{A11}$$

For the Coulomb constitutive law (Equation 5), replacing σ_{nt} in Equation A6 gives

$$\tau_b = \frac{1}{L}\int_L h' N_{loc}dx + \frac{1}{L}\int_L -\mu\sigma_{nn}dx = \frac{1}{L}\int_L (h' N_{loc} + \mu N_{loc})\,dx + (1-s)\mu p_c\,, \tag{A12}$$

with $(1 - s) = L_U/L$ the portion of the bed not drowned by the cavity and over which interfacial drag is non-zero. Rewriting p_c as $\bar{p}_i - N$, we obtain the final bound of C_f for the Coulomb model:

$$C_f \leq \sup(h') + (1-s)\mu + s\mu\bar{p}_i/N\,. \tag{A13}$$

For the N-Coulomb constitutive law (Equation 6) we obtain

$$C_f \leq \sup(h') + \mu, \tag{A14}$$

as suggested by Schoof (2005).

Data Availability Statement

The numerical outputs of the Elmer/Ice simulations and a script to generate Figures 4–6 are accessible in the Zenodo repository of the SAUSSURE project (Gagliardini, 2025).

Acknowledgments
This work was supported by the French National Research Agency project SAUSSURE (ANR-18-CE01-0015-01). OG acknowledges support from the project FricFrac funded by the Center for Advanced Study (CAS) at the Norwegian Academy of Science and Letters during academic year 2023–2024. The authors would like to thank Andrew Fowler, Nathan Maier, Christian Vincent and Ian Hewitt for their useful comments and help. The authors are indebted as well to all reviewers and the editor, whose detailed and insightful comments greatly improved the original manuscript.

References

Alean, P., Braun, S., Iken, A., Schram, K., & Zwosta, G. (1985). Hydraulic effects at the glacier bed and related phenomena (No. 90). *Mitteilungen der Versuchsanstalt für Wasserbau, Hydrologie und Glaziologie*.

Brondex, J., Gillet-Chaulet, F., & Gagliardini, O. (2019). Sensitivity of centennial mass loss projections of the Amundsen Basin to the friction law. *The Cryosphere*, *13*(1), 177–195. https://doi.org/10.5194/tc-13-177-2019

Budd, W. F., Keage, P. L., & Blundy, N. A. (1979). Empirical studies of ice sliding. *Journal of Glaciology*, *23*(89), 157–170. https://doi.org/10.3189/S0022143000029804

Cohen, D., Iverson, N. R., Hooyer, T. S., Fischer, U. H., Jackson, M., & Moore, P. L. (2005). Debris-bed friction of hard-bedded glaciers. *Journal of Geophysical Research*, *110*(2). https://doi.org/10.1029/2004JF000228

Cuffey, K., & Paterson, W. (2010). *The physics of glaciers* (4th ed.). Butterworth-Heinemann.
Doyle, S. H., Hubbard, B., Christoffersen, P., Young, T. J., Hofstede, C., Bougamont, M., et al. (2018). Physical conditions of fast glacier flow: 1. Measurements from boreholes drilled to the bed of store glacier, West Greenland. *Journal of Geophysical Research: Earth Surface*, *123*(2), 324–348. https://doi.org/10.1002/2017JF004529
Fowler, A. C. (1986a). A sliding law for glaciers of constant viscosity in the presence of subglacial cavitation. *Proceedings of the Royal Society of London. A. Mathematical and Physical Sciences*, Vol. 407(1832), 147–170.
Fowler, A. C. (1986b). Sub-temperate basal sliding. *Journal of Glaciology*, *32*(110), 3–5. https://doi.org/10.3189/S0022143000006808
Fowler, A. C. (1987). Sliding with cavity formation. *Journal of Glaciology*, *33*(115), 255–267. https://doi.org/10.3189/s0022143000008820
Gagliardini, O. (2025). Numerical simulation outputs of the paper "impact of interfacial friction at the ice-bed boundary on glacier sliding" by roldan blasco, gimbert, gagliardini and gilbert. *Zenodo*. https://doi.org/10.5281/zenodo.15421627
Gagliardini, O., Cohen, D., Råback, P., & Zwinger, T. (2007). Finite-element modeling of subglacial cavities and related friction law. *Journal of Geophysical Research*, *112*(2). https://doi.org/10.1029/2006JF000576
Gagliardini, O., Zwinger, T., Gillet-Chaulet, F., Durand, G., Favier, L., de Fleurian, B., et al. (2013). Capabilities and performance of Elmer/Ice, a new-generation ice sheet model. *Geoscientific Model Development*, *6*(4), 1299–1318. https://doi.org/10.5194/gmd-6-1299-2013
Gilbert, A., Gimbert, F., Thøgersen, K., Schuler, T. V., & Kääb, A. (2022). A consistent framework for coupling basal friction with subglacial hydrology on hard-bedded glaciers. *Geophysical Research Letters*, *49*(13), e2021GL097507. https://doi.org/10.1029/2021GL097507
Gimbert, F., Gilbert, A., Gagliardini, O., Vincent, C., & Moreau, L. (2021). Do existing theories explain seasonal to multi-decadal changes in glacier basal sliding speed? *Geophysical Research Letters*, *48*(15), 1–10. https://doi.org/10.1029/2021GL092858
Glen, J. W. (1955). The creep of polycrystalline ice. *Proceedings of the Royal Society of London. Series A. Mathematical and Physical Sciences*, Vol. 228(1175), 519–538. https://doi.org/10.1098/rspa.1955.0066
Goelzer, H., Nowicki, S., Payne, A., Larour, E., Seroussi, H., Lipscomb, W. H., et al. (2020). The future sea-level contribution of the Greenland ice sheet: A multi-model ensemble study of ismip6. *The Cryosphere*, *14*(9), 3071–3096. https://doi.org/10.5194/tc-14-3071-2020
Hallet, B. (1979). A theoretical model of glacial abrasion. *Journal of Glaciology*, *23*(89), 39–50. https://doi.org/10.3189/S0022143000029725
Hallet, B. (1981). Glacial abrasion and sliding: Their dependence on the debris concentration in basal ice. *Annals of Glaciology*, *2*, 23–28. https://doi.org/10.3189/172756481794352487
Hansen, D. D., & Zoet, L. K. (2019). Experimental constraints on subglacial rock friction. *Annals of Glaciology*, *60*(80), 37–48. https://doi.org/10.1017/aog.2019.47
Helanow, C., Iverson, N. R., Woodard, J. B., & Zoet, L. K. (2021). Slip laws for bed-bedded glaciers derived from actual bed topography. *Science Advances*, *7*(May), 2–10. https://doi.org/10.1126/sciadv.abe7798
Helanow, C., Iverson, N. R., Zoet, L. K., & Gagliardini, O. (2020). Sliding relations for glacier slip with cavities over three-dimensional beds. *Geophysical Research Letters*, *47*(3). https://doi.org/10.1029/2019GL084924
Helmstetter, A., Nicolas, B., Comon, P., & Gay, M. (2015). Basal icequakes recorded beneath an alpine glacier (Glacier d'Argentière, Mont Blanc, France): Evidence for stick-slip motion? *Journal of Geophysical Research: Earth Surface*, *120*(3), 379–401. https://doi.org/10.1002/2014JF003288
Hooke, R. L., Pohjola, V. A., Jansson, P., & Kohler, J. (1992). Intra-seasonal changes in deformation profiles revealed by borehole studies, Storglaciaren, Sweden. *Journal of Glaciology*, *38*(130), 348–358. https://doi.org/10.1017/S0022143000002239
Iken, A. (1981). The effect of the subglacial water pressure on the sliding velocity of a glacier in an idealized numerical model. *Journal of Glaciology*, *27*(97), 407–421. https://doi.org/10.3189/S0022143000011448
Iverson, N. R., Cohen, D., Hooyer, T. S., Fischer, U. H., Jackson, H., Moore, P. L., et al. (2003). Effects of basal debris on glacier flow. *Science*, *301*(5629), 81–84. https://doi.org/10.1126/science.1083086
Iverson, N. R., Helanow, C., & Zoet, L. K. (2019). Debris-bed friction during glacier sliding with ice-bed separation. *Annals of Glaciology*, *60*(80), 30–36. https://doi.org/10.1017/aog.2019.46
Jaeger, J., Cook, N., & Zimmerman, R. (2007). *Fundamentals of rock mechanics*. Wiley.
Köpfli, M., Gräff, D., Lipovsky, B. P., Selvadurai, P. A., Farinotti, D., & Walter, F. (2022). Hydraulic conditions for stick-slip tremor beneath an alpine glacier. *Geophysical Research Letters*, *49*(21), 1–11. https://doi.org/10.1029/2022gl100286
Lipovsky, B. P., Meyer, C. R., Zoet, L. K., McCarthy, C., Hansen, D. D., Rempel, A. W., & Gimbert, F. (2019). Glacier sliding, seismicity and sediment entrainment. *Annals of Glaciology*, *60*(79), 182–192. https://doi.org/10.1017/aog.2019.24
Lliboutry, L. (1959). Une théorie du frottement du glacier sur son lit. *Annales de Geophysique*, *15*, 250.
Lliboutry, L. (1968). General theory of subglacial cavitation and sliding of temperate glaciers. *Journal of Glaciology*, *7*(49), 21–58. https://doi.org/10.3189/s0022143000020396
Maier, N., Humphrey, N., Harper, J., & Meierbachtol, T. (2019). Sliding dominates slow-flowing margin regions, Greenland ice sheet. *Science Advances*, *5*(7), eaaw5406. https://doi.org/10.1126/sciadv.aaw5406
Mantelli, E., Haseloff, M., & Schoof, C. (2019). Ice sheet flow with thermally activated sliding. Part 1: The role of advection. *Proceedings of the Royal Society A*, *475*(2230), 20190410. https://doi.org/10.1098/rspa.2019.0410
McCarthy, C., Savage, H., & Nettles, M. (2017). Temperature dependence of ice-on-rock friction at realistic glacier conditions. *Philosophical Transactions of the Royal Society A: Mathematical, Physical and Engineering Sciences*, *375*(2086), 20150348. https://doi.org/10.1098/rsta.2015.0348
Morland, L. W. (1976). Glacier sliding down an inclined wavy bed with friction. *Journal of Glaciology*, *17*(77), 463–477. https://doi.org/10.3189/S0022143000013745
Robin, G. D. (1976). Is the basal ice of a temperate glacier at the pressure melting point? *Journal of Glaciology*, *16*(74), 183–196. https://doi.org/10.3189/S002214300003152X
Roeoesli, C., Helmstetter, A., Walter, F., & Kissling, E. (2016). Meltwater influences on deep stick-slip icequakes near the base of the Greenland ice sheet. *Journal of Geophysical Research: Earth Surface*, *121*(2), 223–240. https://doi.org/10.1002/2015JF003601
Roldán-Blasco, J.-P., Gilbert, A., Piard, L., Gimbert, F., Vincent, C., Gagliardini, O., et al. (2025). Creep enhancement and sliding in a temperate, hard-bedded alpine glacier. *The Cryosphere*, *19*(1), 267–282. https://doi.org/10.5194/tc-19-267-2025
Röthlisberger, H. (1972). Water pressure in intra and subglacial channels. *Journal of Glaciology*, *11*(62), 177–203. https://doi.org/10.3189/S0022143000022188
Schoof, C. (2005). The effect of cavitation on glacier sliding. *Proceedings of the Royal Society A: Mathematical, Physical and Engineering Sciences*, Vol. 461(2055), 609–627. https://doi.org/10.1098/rspa.2004.1350
Schulson, E. M., & Duval, P. (2009). Creep and fracture of ice. https://doi.org/10.1017/CBO9780511581397
Schweizer, J., & Iken, A. (1992). The role of bed separation and friction in sliding over an undeformable bed. *Journal of Glaciology*, *38*(128), 77–92. https://doi.org/10.1017/S0022143000009618

Seroussi, H., Nowicki, S., Payne, A. J., Goelzer, H., Lipscomb, W. H., Abe Ouchi, A., et al. (2020). Ismip6 Antarctica: A multi-model ensemble of the antarctic ice sheet evolution over the 21 st century. *The Cryosphere Discussions*, *2020*(9), 1–54. https://doi.org/10.5194/tc-14-3033-2020

Thøgersen, K., Gilbert, A., Schuler, T. V., & Malthe-Sørenssen, A. (2019). Rate-and-state friction explains glacier surge propagation. *Nature Communications*, *10*(1), 2823. https://doi.org/10.1038/s41467-019-10506-4

Thompson, A. C., Iverson, N. R., & Zoet, L. K. (2020). Controls on subglacial rock friction: Experiments with debris in temperate ice. *Journal of Geophysical Research: Earth Surface*, *125*(10), 1–18. https://doi.org/10.1029/2020JF005718

Togaibekov, A., Gimbert, F., Gilbert, A., & Walpersdorf, A. (2024). Observing and modeling short-term changes in basal friction during rain-induced speed-ups on an alpine glacier. *Geophysical Research Letters*, *51*(14), e2023GL107999. https://doi.org/10.1029/2023GL107999

Weertman, J. (1957). On the sliding of glaciers. *Journal of Glaciology*, *3*(21), 33–38. https://doi.org/10.3189/s0022143000024709

Wiens, D. A., Anandakrishnan, S., Winberry, J. P., & King, M. A. (2008). Simultaneous teleseismic and geodetic observations of the stick-slip motion of an Antarctic ice stream. *Nature*, *453*(7196), 770–774. https://doi.org/10.1038/nature06990

Zoet, L. K., Anandakrishnan, S., Alley, R. B., Nyblade, A. A., & Wiens, D. A. (2012). Motion of an Antarctic glacier by repeated tidally modulated earthquakes. *Nature Geoscience*, *5*(9), 623–626. https://doi.org/10.1038/ngeo1555

Zoet, L. K., Carpenter, B., Scuderi, M., Alley, R. B., Anandakrishnan, S., Marone, C., & Jackson, M. (2013). The effects of entrained debris on the basal sliding stability of a glacier. *Journal of Geophysical Research: Earth Surface*, *118*(2), 656–666. https://doi.org/10.1002/jgrf.20052

Zoet, L. K., & Iverson, N. R. (2015). Experimental determination of a double-valued drag relationship for glacier sliding. *Journal of Glaciology*, *61*(225), 1–7. https://doi.org/10.3189/2015JoG14J174